A Structural Model for the Osmosensor, Transporter, and Osmoregulator ProP of *Escherichia coli*†

Janet M. Wood,*,‡ Doreen E. Culham,‡ Alexander Hillar,§ Yaroslava I. Vernikovska,§ Feng Liu,§ Joan M. Boggs,§ and Robert A. B. Keates‡

Department of Molecular and Cellular Biology and Guelph-Waterloo Centre for Graduate Work in Chemistry and Biochemistry, University of Guelph, Guelph N1G 2W1, Ontario, Canada, Department of Structural Biology and Biochemistry, Hospital for Sick Children, Toronto M5G 1X8, Ontario, Canada, and Department of Laboratory Medicine and Pathobiology, University of Toronto, Toronto M5G 1L5, Ontario, Canada

Received December 13, 2004; Revised Manuscript Received February 4, 2005

ABSTRACT: Transporter ProP of *Escherichia coli*, a member of the major facilitator superfamily (MFS), acts as an osmosensor and an osmoregulator in cells and after purification and reconstitution in proteoliposomes. H^+-osmoprotectant symport via ProP is activated when medium osmolality is elevated with membrane impermeant osmolytes. The three-dimensional structure of ProP was modeled with the crystal structure of MFS member GlpT as a template. This GlpT structure represents the inward (or cytoplasm)-facing conformation predicted by the alternating access model for transport. LacZ−PhoA fusion analysis and site-directed fluorescence labeling substantiated the membrane topology and orientation predicted by this model and most hydropathy analyses. The model predicts the presence of a proton pathway within the N-terminal six-helix bundle of ProP (as opposed to the corresponding pathway found within the C-terminal helix bundle of its paralogue, LacY). Replacement of residues within the N-terminal helix bundle impaired the osmotic activation of ProP, providing the first indication that residues outside the C-terminal domain are involved in osmosensing. Some residues that were accessible from the periplasmic side, as predicted by the structural model, were more susceptible to covalent labeling in permeabilized membrane fractions than in intact bacteria. These residues may be accessible from the cytoplasmic side in structures not represented by our current model, or their limited exposure in vivo may reflect constraints on transporter structure that are related to its osmosensory mechanism.

Cells respond to changes in extracellular osmolality by modulating their cytoplasmic composition. Osmoregulatory transporters and biosynthetic enzymes mediate solute accumulation as osmolality increases. Mechanosensitive channels mediate solute release as osmolality decreases. Archaea (*1*, *2*), eubacteria (*3*, *4*), and eukaryotic cells (*5*−*10*) share these responses.

Osmoprotectants are organic solutes that stimulate microbial growth in high-osmolality media. They act as or are converted to compatible solutes, compounds that can accumulate to high cytoplasmic levels without impairing cellular function. Three osmoprotectant transporters have been expressed, purified, and reconstituted into proteoliposomes: major facilitator superfamily (MFS)[1] member ProP of *Escherichia coli* (*11*), betaine-carnitine-choline transporter (BCCT) family member BetP of *Corynebacterium glutamicum* (*12*), and ATP binding cassette (ABC) transporter OpuA of *Lactococcus lactis* (*13*). Each can sense and respond to osmolality changes in the absence of other proteins. The proteoliposome systems provide new opportunities to elucidate the osmosensory mechanisms of these transporters (*3*, *14*−*16*), each representing a ubiquitous class of molecules that forestall the dehydration of animal, plant, and microbial cells by mediating the uptake of organic solutes.

ProP (TC number 2.A.1.6.4) is a 500-residue integral membrane protein (*17*) and a H^+-osmoprotectant symporter

† This work was supported by Research Grants MOP-42463, IG1-67335, and MOP-68904 awarded to J.M.W. and J.M.B. by the Canadian Institutes of Health Research, a Postdoctoral Fellowship awarded to A.H. by the Natural Sciences and Engineering Research Council of Canada, and a postdoctoral fellowship awarded to F.L. by the Hospital for Sick Children-Research Training Centre.

* To whom correspondence should be addressed: Department of Molecular and Cellular Biology, University of Guelph, Guelph, ON N1G 2W1, Canada. Telephone: (519) 824-4120, ext. 53866. Fax: (519) 837-1802. E-mail: jwood@uoguelph.ca.

‡ University of Guelph.

§ Hospital for Sick Children and University of Toronto.

[1] Abbreviations: 3D-PSSM, three-dimensional position-specific scoring matrix; ΔΨ, membrane potential; ABC transporter, ATP binding cassette transporter; BCCT family, betaine−carnitine−choline transporter family; DNase I, deoxyribonuclease I; EDTA, ethylenediaminetetraacetic acid; IPTG, isopropyl β-D-thiogalactopyranoside; LacZ, β-galactosidase; LB, Luria−Bertani medium; MEMSAT, membrane protein structure and topology; MFS, major facilitator superfamily; MOPS, 4-morpholinopropanesulfonic acid; MTS, methanethiosulfonate; MTSEA, 2-(aminoethyl)methanethiosulfonate; MTSES, 2-(sulfonatoethyl)methanethiosulfonate; MTSET, methanethiosulfonate-ethyltrimethylammonium; OGM, Oregon green 488 maleimide carboxylic acid; oNP, *o*-nitrophenol; oNPG, *o*-nitrophenyl β-D-galactopyranoside; PhoA, alkaline phosphatase; PAGE, polyacrylamide gel electrophoresis; PCR, polymerase chain reaction; pNP, *p*-nitrophenol; pNPP, *p*-nitrophenyl phosphate; rms, root-mean-square; SDS, sodium dodecyl sulfate; SPDBV, Swiss Protein Database Viewer; TC, transporter classification; TM, transmembrane segment (a sequence of amino acids that extends from one membrane surface to the other in an integral membrane protein); XG, 5-bromo-4-chloro-3-indolyl β-D-galactoside; XP, 5-bromo-4-chloro-3-indolyl phosphate.

10.1021/bi047383o CCC: $30.25
Published on Web 03/25/2005

powered by both ΔpH and ΔΨ (*18*−*20*). Its many substrates, all highly water-soluble zwitterions with no net charge, include proline, glycine betaine, and ectoine (*19*). The initial rate of proline uptake via ProP is a sigmoid function of osmolality (not osmotic shift) in both cells and proteoliposomes (*21*). ProP is an osmosensor because chemically diverse, membrane impermeant osmolytes contribute to its activation as they contribute to the osmolality of the external medium (*21*). The same is true of BetP and OpuA (*16*). However, in proteoliposomes, all three systems respond in an osmolyte-specific manner to the lumenal solvent (*21*−*24*). Thus, the semipermeable membrane transduces the extracellular, osmotic signal to yield a cytoplasmic signal which may be osmosensor-specific (*16*, *21*, *24*).

Although ProP can undergo osmotic activation in the absence of other proteins, soluble protein ProQ amplifies the osmotic activation of ProP in vivo (*25*, *26*). ProQ has been modeled as a two-domain protein in which an α-helical N-terminal domain (residues 1−124) and an SH3-like C-terminal domain (residues 179−232) are connected by an unstructured linker (*27*). ProQ may act directly on ProP since *proQ* lesions alter neither *proP* transcription nor ProP protein levels (*25*, *26*).

ProP, BetP, and OpuA sense, transduce, and respond to osmotic signals. To understand osmosensing, we must correlate the structural dynamics of these proteins with osmoregulation of their transport activities. Like other integral membrane proteins, MFS members have long proven to be refractory to crystallization and X-ray structure determination (*28*−*30*). At last, structures have been reported for the oxalate:formate antiporter OxlT of *Oxalobacter formigenes* (*31*) at 3.4 Å resolution (two dimensions only) and for the glycerol-3-phosphate:phosphate antiporter GlpT (*32*) and the H^+-lactose symporter LacY (*33*) of *E. coli* (resolutions of 3.3 and 3.5 Å, respectively). They reveal shared characteristics (*34*) that distinguish these MFS members from other membrane proteins, including the archetype, bacteriorhodopsin. Most notably, the transmembrane helices are variable in length, highly kinked, and braided with each other. Some begin in contact with the lipid, disappear into the interior of the protein, and finally emerge, exposed to the periplasm or cytoplasm (e.g., helices IV and X). Since some extend beyond the membrane surface, only part displays the hydrophobic characteristics previously expected of a TM, and that part may appear to be too short to traverse a phospholipid bilayer. The fact that MFS members share a common fold (*34*) led us to use them as templates in modeling *E. coli* ProP. Here we report functional insights gained from the resulting structural model.

Prior to direct, high-resolution structure determination, techniques were developed which support indirect structural analyses for this class of integral membrane proteins (*35*). Two of these techniques have been used to begin evaluation of our structural model of ProP: (1) isolation of hybrid proteins in which an N-terminal ProP fragment directs marker enzyme LacZ (β-galactosidase) or PhoA (alkaline phosphatase) to the cytoplasm or periplasm, respectively, and (2) site-directed fluorescent labeling of cysteine (Cys) residues introduced into putative cytoplasmic or periplasmic loops or termini. The resulting data are consistent with our structural model, and in turn suggest new models for osmosensing and the osmoregulation of ProP activity.

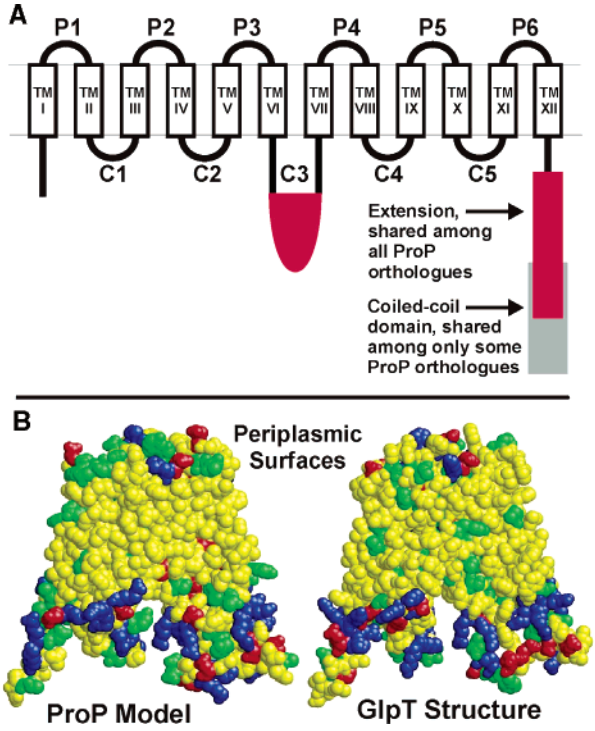

FIGURE 1: Structural models of ProP. (A) Schematic representation. ProP is predicted to form a series of transmembrane (TM) α-helices linked by hydrophilic loops (periplasmic loops P1−P6 and cytoplasmic loops C1−C5), with hydrophilic N- and C-terminal domains. The membrane topology and orientation of ProP were analyzed using a variety of algorithms (*51*). All predicted similar locations for putative transmembrane helices VI−XII, a cytoplasmic C-terminus, and a particularly long loop C3 (colored red). The positions of helices I−V were less obvious. One algorithm (TOPPRED) predicted a structure that lacked TMI and had a periplasmic N-terminus. This paper confirms that ProP is comprised of 12 TMs and has cytoplasmic N- and C-termini. The C-terminal domain of *E. coli* ProP is approximately 55 amino acids longer than those of its paralogues (*17*). Two classes of ProP orthologues are observed (*16*). The C-terminal domains of orthologues typified by *E. coli* ProP terminate in a sequence with heptad repeats characteristic of α-helical coiled coil-forming proteins (gray box, 30−37 amino acids). The C-terminal domains of orthologues typified by *C. glutamicum* ProP (*71*) are shorter and do not share the heptad repeats characteristic of coiled coil-forming proteins (red box, 35−47 amino acids). (B) Crystal structure of GlpT (right) and derived model of ProP (left): yellow for hydrophobic residues, green for polar uncharged residues, blue for positively charged residues, and red for negatively charged residues. ProP residues 1−4, 236−246 (part of loop C3, red in schematic diagram above), and 453−500 (red and gray in the schematic) are not represented by this model. The NMR structure of the antiparallel coiled coil formed by a peptide replica of residues 468−497 (gray in the schematic) is known (PDB entry 1R48) (*37*).

Extensive structure−function analyses have implicated an α-helical coiled-coil domain at the cytoplasmic, C-terminus of *E. coli* ProP in the osmoregulation of ProP activity (*17*, *36*−*38*). The C-terminus of ProP is longer than those of its closest paralogues that are not osmosensors or osmoregulators (KgtP and ShiA) (gray rectangle in Figure 1A) (*17*). A peptide corresponding to the ProP C-terminus forms an antiparallel, homodimeric α-helical coiled coil (*36*, *37*). This structure is also present in full-length ProP, in vivo (A. P. Hillar, D. E. Culham, Ya. I. Vernikovska, J. M. Wood, and J. M. Boggs, unpublished data). Structural modifications that impair formation of the coiled coil also elevate the osmolality threshold for ProP activation (*36*; Y. Tsatskis and J. M.

Wood, unpublished data). Deletion analysis has implicated an extended, cytoplasmic C-terminal domain in osmosensing by BetP (*39*), but the three-dimensional structure of that domain is not known. Recent genomic sequencing has revealed groups of ProP orthologues that do and do not include the coiled-coil structure, though all have extended C-termini (red rectangle in Figure 1A). Representatives of both groups share similar osmosensory and osmoregulatory functions (*16*; Y. Tsatskis and J. M. Wood, unpublished data). Thus, the C-terminal coiled coil is not essential for osmosensing or osmotic activation, but it modulates the sensitivity of ProP to medium osmolality. This paper reports the first evidence that other parts of ProP are relevant to its role as an osmosensor.

EXPERIMENTAL PROCEDURES

Structure Prediction and Comparative Modeling. ProP secondary structure was predicted by combining results from PsiPred (*40*) and JPred (*41*). Secondary structures of template proteins GlpT (*32*) and LacY (*33*) were taken from their Protein Data Bank entries (1PW4 for GlpT and 1PV6 and 1PV7 for LacY) and were verified by inspection of the hydrogen bonding patterns in the structure. Transmembrane helices and topology were predicted by MEMSAT (*42*). CLUSTAL W (*43*) was used to derive multiple-sequence alignments of ProP homologues from 51 prokaryotic species. In addition, the multiple-sequence alignment of paralogues KgtP, ProP, ShiA, LacY, and GlpT was correlated with their predicted or actual secondary structure and transmembrane topology. Surface exposure of side chains contacting the lipid acyl chains in GlpT and LacY was mapped in SPDBV (*44*).

The 3D-PSSM web server (*45*) was used to construct initial sequence-to-structure alignments among ProP, GlpT, and LacY. These alignments were then refined by hand to position insertions or deletions in the exposed surface loops rather than within helical segments, and further refined to align nonpolar side chains in bilayer-exposed positions in the ProP model. Models were then constructed in SPDBV (*44*). SPDBV was also used for side chain replacement and rotamer optimization, energy minimization, calculating electrostatic potential surfaces, and superimposition of structures.

Materials and Culture Media. Bovine pancreatic DNase I (type II) was from Boehringer-Mannheim (Laval, PQ). Egg white lysozyme (UltraPure grade) was obtained from Caledon Laboratories (Georgetown, ON). Oligonucleotides were purchased from Cortec DNA Services (Kingston, ON), Oregon green 488 maleimide carboxylic acid (OGM) was purchased from Molecular Probes Inc. (Eugene, OR). Ampicillin, β-mercaptoethanol, imidazole, *o*-nitrophenyl β-D-galactopyranoside (oNPG), *o*-nitrophenol (oNP), *p*-nitrophenyl phosphate (pNPP), and *p*-nitrophenol (pNP) were from Sigma Chemical Co. (St. Louis, MO). 2-(Aminoethyl)-methanethiosulfonate (MTSEA), 2-(sulfonatoethyl)methanethiosulfonate (MTSES), and methanethiosulfonate ethyltrimethylammonium (MTSET) were purchased from Toronto Research Chemicals Inc. (Toronto, ON). OGM, MTSEA, MTSES, and MTSET were prepared as stock solutions in *N*,*N*-dimethylformamide (Fisher Scientific Inc., Nepean, ON) and stored at −20 °C, protected from light, prior to use. Other reagents were of the highest grade available. Buffers were prepared as described by Racher et al. (*20*), and solution osmolalities were measured with a Wescor vapor pressure osmometer (Wescor, Logan, UT).

Bacteria were cultivated at 37 °C in LB (*46*) or in NaCl-free MOPS medium, a variant of the MOPS medium described by Neidhardt et al. (*47*) from which all NaCl had been omitted. This base medium was supplemented with NH_4Cl (9.5 mM) as a nitrogen source and glycerol [0.4% (v/v)] as a carbon source. L-Tryptophan (245 μM) and thiamine hydrocholoride (1 μg/mL) were added to meet auxotrophic requirements, creating a complete growth medium with an osmolality of 0.14−0.15 mol/kg. Ampicillin (100 μg/mL) was added as required to maintain plasmids.

Bacteria, Plasmids, and Molecular Biological Manipulations. Basic molecular biological techniques were as described by Sambrook et al. (*48*), and the polymerase chain reaction (PCR) was carried out as described by Brown and Wood (*49*). Genes encoding ProP and its variants were expressed from the AraC-controlled P_{BAD} promoter in plasmid-bearing derivatives of *E. coli* WG350 [F$^-$ *trp lacZ rpsL thi* Δ(*putPA*)*101* Δ(*proU*)*600* Δ(*proP-melAB*)*212*] (*17*). Each strain contained plasmid pDC79 [a derivative of pBAD24 (*50*) encoding wild-type ProP (*36*)], pDC80 [a derivative of pBAD24 encoding ProP-His_6 (*20*)], pDC117 [a derivative of pBAD24 encoding the fully functional cysteine-less variant of ProP-His_6 with amino acid replacements C112A, C133A, C264V, and C367A, denoted ProP* (*51*)], or a derivative of one of those plasmids. Plasmids encoding these variants were created by site-directed mutagenesis as previously described (*51*).

Creation and Analysis of ProP′::′PhoA and ProP′::′LacZ Fusions. Banks of plasmids encoding diverse ProP′::′PhoA or ProP′::′LacZ fusions were constructed and screened to identify those conferring alkaline phosphatase (PhoA) or β-galactosidase (LacZ) activity as described by Daniels et al. (*52*) using indicator media supplemented with 5-bromo-4-chloro-3-indolyl phosphate (XP, 40 or 80 μg/mL) or 5-bromo-4-chloro-3-indolyl β-D-galactoside (XG, 40 μg/mL), respectively. The full-length *proP*::′*phoA* fusion encoding the protein (ProP-E500)-WIPRAAGIRYQAYRYRR-(P27-PhoA) was created by PCR-amplifying *proP* with flanking *Xba*I and *Bam*HI sites, cleaving, and inserting it at the corresponding sites within vector pRMCD28 (*52*). The full-length *proP*::′*lacZ* fusion encoding the protein (ProP-E500)-SAGIPGDP-(V8-LacZ) was created by PCR-amplifying *proP* with flanking *Xba*I and *Pst*I sites and inserting it at the corresponding sites within vector pRMCD70 (*52*). Plasmids encoding proteins with nested, unidirectional deletions of the ProP C-terminus were made using the Erase-a-Base kit (Promega,) as described previously (*52*). The ′PhoA-encoding plasmid was prepared for directed exonuclease III digestion by cleavage with *Pst*I and *BamH*I. The ′LacZ-encoding plasmid was prepared by cleavage with *Bam*HI, treatment with the Klenow fragment of DNA polymerase in the presence of phosphorothioate nucleotides, and subsequent cleavage with *Eco*RI. The resulting plasmid banks were transformed into *E. coli* DH5α [F$^-$ ϕ80 d*lacZ*ΔM15 Δ(*lacZYA-argF*)U169 *recA1 endA1 hsdR17* (r_k^- m_k^+) *supE44* λ^- *thi-1 gyrA relA1*] (*53*), and bacteria expressing fusion proteins with indicator enzyme activity were identified as described above. They were then screened by restriction analysis to identify representative fusions, and the fusion joints were located by DNA sequence analysis performed

by the Laboratory Services Division, University of Guelph.

Transport and Enzyme Assays. Published procedures were used to cultivate bacteria in NaCl-free MOPS medium and to assess proline uptake via ProP (*21*). The expression levels of ProP-His_6 and its variants in intact bacteria were determined as previously described (*36*).

PhoA and LacZ activities were measured using a modification of the procedure described by Daniels et al. (*52*). Bacteria were cultivated in LB medium (*46*) (2 mL) supplemented with ampicillin overnight and subcultured (5%, v/v) in LB medium with ampicillin and isopropyl β-D-thiogalactopyranoside (IPTG) (40 μg/mL). IPTG was added to induce expression of the genes encoding the fusion proteins from the *lac* promoter of vectors pRMCD28 and pRMCD70 (*52*). The cultures were incubated, while being shaken, at 37 °C for 1.75 h until the optical density (600 nm) reached approximately 0.8. Cells were harvested by centrifugation at 4 °C, washed with an equal volume of cold A buffer [PhoA assays, 10 mM Tris-HCl and 10 mM $MgSO_4$ (pH 8)] or Z buffer [LacZ assays, 60 mM Na_2HPO_4, 40 mM NaH_2PO_4, 10 mM KCl, and 1 mM $MgSO_4$ (pH 7)] and resuspended in an equal volume of 1 M Tris-HCl (pH 8) (PhoA assays) or Z buffer (LacZ assays). Three milliliters of the resulting suspension was mixed with sodium dodecyl sulfate (150 μL, 1 mg/mL) and chloroform (150 μL), vortexed for 10 s, and then incubated at 28 °C for 5 min. Eight aliquots (200 μL) were delivered to the wells of a microtiter plate, and quench reagent was added to four of them (40 μL of 1 M K_2HPO_4 for PhoA or 2 M Na_2CO_3 for LacZ). The substrates (40 μL, added to all eight wells) were *p*-nitrophenyl phosphate [pNPP, 15 mM in 1 M Tris-HCl (pH 8)] for PhoA and *o*-nitrophenyl galactoside (ONPG, 13.3 mM in Z buffer) for LacZ. These reaction mixtures were incubated at 28 °C until adequate color had developed; the appropriate quench reagents were added to the remaining wells, and absorbances (405 nm) were determined for assay mixtures, prequenched controls, and standard product solutions [*p*-nitrophenyl phosphate (pNPP) for PhoA and *o*-nitrophenyl phosphate (oNPP) for LacZ]. The mean absorbances of the assay mixtures were corrected by subtracting the mean absorbances of the prequenched controls. The enzyme activities are expressed as nanomoles of product per minute per absorbance unit [an absorbance unit being the absorbance (600 nm) of the cell suspension prepared for each assay, corrected for dilution in the assay mixture]. The background alkaline phosphatase activity, obtained with *E. coli* DH5α and with that strain expressing the ProP-E500::PhoA fusion, was 0 nmol min^{-1} $A_{600}{}^{-1}$. The background β-galactosidase activity, obtained with *E. coli* DH5α, was -67 nmol min^{-1} $A_{600}{}^{-1}$. This negative value arose because the rate of spontaneous hydrolysis of substrate ONPG after addition of the quench reagent was higher than the corresponding rate in the assay buffer.

The expression levels of ProP′::′PhoA and ProP′::′LacZ fusion proteins were determined by Western blotting of proteins extracted from the cells prepared for enzyme assays (see above). Western blotting was performed as previously described (*36*) except that 8−16% Tris-glycine gels (Invitrogen Life Technologies, Carlsbad, CA) were used to facilitate resolution of the expected, high-molecular mass fusion proteins (molecular mass ranges of 50−100 and 100−150 kDa for the ProP′::′PhoA and ProP′::′LacZ fusions, respectively). Rabbit anti-*E. coli* alkaline phosphatase (Polysciences, Warrington, PA) and mouse anti-*E. coli* β-galactosidase (Sigma-Aldrich Corp., St. Louis, MO) were used as primary antibodies with goat anti-rabbit or anti-mouse IgG conjugated to horseradish peroxidase (Jackson ImmunoResearch Laboratories, West Grove, PA) as the secondary antibody. The anti-*E. coli* alkaline phosphatase was purified by affinity chromatography using a column prepared by coupling purified *E. coli* alkaline phosphatase (Sigma-Aldrich Corp.) to cyanogen bromide-activated Sepharose 4 Fast Flow (Amersham Biosciences, Piscataway, NJ) as described by the manufacturer of the column matrix. Separate gels were silver stained (SilverXpress Silver Staining Kit, Invitrogen Life Technologies) to control for protein loading.

Site-Directed Fluorescence Labeling. The cytoplasmic or periplasmic exposure of cysteine residues in ProP*-His_6 variants was determined by site-directed fluorescence labeling of cells and membranes, with and without prior blockage by MTS reagents (0.2 mM) added to cells, as previously described (*51*). The membranes were permeabilized by freezing and thawing in the presence of OGM. Variants that were not labeled well by OGM in cells or membranes were labeled in a SDS solution as described previously (*51*). Cells were or were not treated with MTS reagents as specified in the Results; ProP variants were purified, eluted in buffer containing 2% SDS, and then labeled with OGM.

RESULTS

A Structural Model for ProP. To create a structural model for ProP, we exploited the most closely related sequences for paralogues of known function [ShiA, a proton-shikimate symporter (30% identical), and KgtP, a proton-α-ketoglutarate symporter (28% identical)] as well as the sequences and crystal structures of paralogues GlpT (17% identical) and LacY (16% identical). ProP was aligned with the sequences of LacY and GlpT by two different methods. The multiple-sequence alignment of ShiA, ProP, KgtP, LacY, and GlpT was generated with Clustal W. This alignment shows few gaps, and the predicted transmembrane segments (TMs) in KgtP, ProP, and ShiA correlate well with actual boundaries in the crystal structures of LacY and GlpT (Figure 1S of the Supporting Information). Alignments were also generated by 3D-PSSM, which matches sequences by structural propensity in addition to sequence similarity. 3D-PSSM (with global-local option) recorded GlpT (1PW4) as the strongest match ($E = 2.98 \times 10^{-5}$), with a theoretical model of the human facilitative glucose transporter GLUT1 [1JA5 (*54*)] second and LacY (1PV7) third ($E = 6.53 \times 10^{-3}$). The global-local option eliminates the penalty for the C-terminal coiled-coil domain of ProP, which is not matched in either GlpT or LacY.

Sequence correlations among ProP, LacY, and GlpT are concentrated in small islands, in particular, the MFS signature motif [RK]-x-x-[RK]-[RK], found in loops C1 and C4 (Figures 1 and 2). These serve to anchor the alignment at key points, leaving large regions where the level of sequence identity is below average, and where random matches can provide potentially misleading alignments. As would be true for other integral membrane proteins with minimal hydrophilic domains, randomized sequences containing the amino acid composition of ProP, which is biased toward hydro-

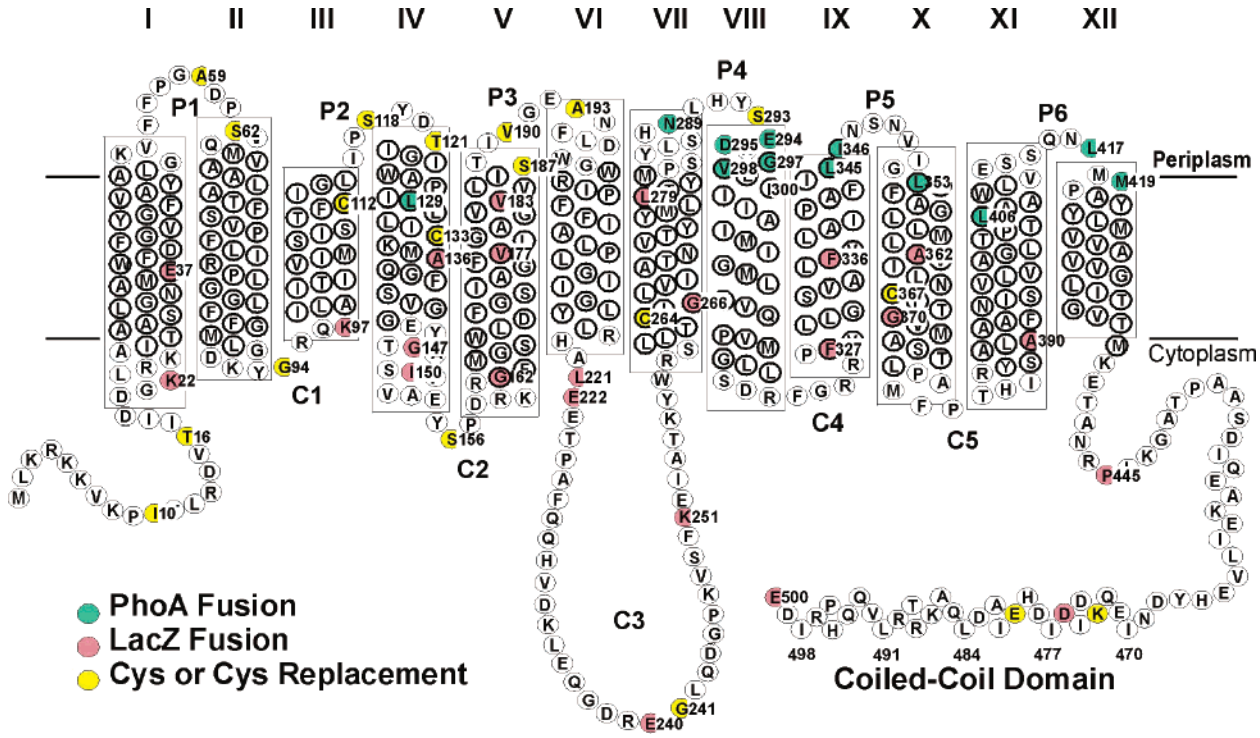

FIGURE 2: Experimental analysis of the ProP structure. The diagram shows a secondary structure model of ProP derived as follows. Boxes enclose the membrane-spanning α-helices predicted by our structural model (Figure 1B). Bold circles mark residues predicted to be in TMs (between the membrane surfaces) by MEMSAT (*42*). Horizontal lines represent the approximate locations of the membrane surfaces (see the text). Plasmids encoding ProP′::′PhoA and ProP′::′LacZ fusions were created and analyzed as described in Experimental Procedures. The positions of these fusions are marked by green and pink circles, respectively. The marker enzyme activities of the fusion proteins are reported in Table 2, and the expression levels of the ProP′::′PhoA fusion proteins are illustrated in Figure 3. Yellow circles mark the positions of cysteine (Cys) residues, available in the background of the Cys-less variant ProP* (*51*), that served as targets for membrane impermeant, fluorescent reagent Oregon green maleimide (OGM) and MTS reagents as described previously (*51*). The expression levels and proline uptake activities of these variants are reported in Figures 4 and 5, respectively.

Table 1: Relative Abundance of Amino Acids and Exposure to Lipid Acyl Chains[a]

residue	GlpT overall	GlpT acyl chains	LacY overall	LacY acyl chains	ProP overall	ProP acyl chains
A	45	10	35	5	47	11
C	7	2	7	1	4	1
D	14	0	6	0	22	0
E	14	0	11	0	18	0
F	33	21	56	21	29	12
G	45	5	37	7	43	3
H	7	0	4	0	9	0
I	31	17	33	14	48	22
K	16	0	12	0	20	0
L	50	19	54	27	60	28
M	22	9	14	7	19	6
N	12	0	16	0	11	0
P	25	0	12	2	23	4
Q	10	0	11	0	14	0
R	17	0	12	0	19	0
S	20	2	29	2	26	3
T	15	3	19	4	25	4
V	32	16	29	15	39	16
W	15	6	6	3	7	2
Y	22	4	14	1	17	3
total	452	114	417	109	500	115

[a] The surface exposure of side chains was calculated with SPDBV (*44*).

phobic residues (Table 1), align with as much as 15% residue identity. On this basis, we treated matches of less abundant polar amino acids as more significant than matches of high-abundance nonpolar side chains.

Figure 1S of the Supporting Information shows the locations of the predicted TMs. For the two crystal structures, GlpT (1PW4) and LacY (1PV7), the side chains that are believed to directly contact the lipid acyl chains of the bilayer (*32*, *33*) are shown in pink. Table 1 shows that A, F, I, L, M, V, and W are most likely to be in contact with the lipid acyl chains, with minor contributions from C, G, P, S, T, and Y. Strongly polar amino acids are totally excluded. Where present within the bilayer core, the side chains of S, T, and Y were only partly exposed to the lipid acyl chains and were generally positioned to allow hydrogen bonding to the helix backbone or adjacent helices. The helices of GlpT and LacY contain many kinks and irregularities, and do not always conform to the canonical 3.6 amino acids per helix turn. As a result, the pattern of side chains in contact with lipid acyl chains is frequently out of phase with that expected from a purely sequence-based alignment of GlpT and LacY (see TMs III, VIII, and IX in Figure 1S of the Supporting Information). On this basis, we considered it appropriate to fine-tune the alignment of ProP to the template so that the population of side chains in lipid contact would conform to the distributions seen in Table 1. This was done by aligning each TM to optimize the exposure of the appropriate residues while minimizing total insertions and deletions. Most gaps are found at the terminal loops. Occasionally, regular α-helical structure and hydrogen bonding may be interrupted by including a non-H-bonded kink, or a loop of 3_{10} or π helix, in which case it may be justified to insert or delete one residue in midhelix. Such a deletion appears in the

machine-generated alignment in TM IX (Figure 1S of the Supporting Information).

Several possible alignments of ProP with each template (LacY or GlpT) were derived. Of these, one alignment of ProP with GlpT was chosen for modeling because it showed the best overall distribution of recognizable sequence matches, and gave a significantly better *E* score in 3D-PSSM. The final optimized alignment is shown in Figure 2S of the Supporting Information. From this alignment, the GlpT crystal structure was used as the template to build the ProP model shown in Figure 1B. The resulting model (Protein Data Bank entry 1Y8S) shows the characteristic belt of nonpolar residues, with a concentration of positively charged residues at the cytoplasmic membrane boundary. The latter is seen even though there is only partial correspondence of positive amino acids in the aligned sequences. As in the GlpT structure, helices I, IV, VII, and X line a putative organic substrate pore to which flanking helices II, V, VIII, and XI also contribute. Helices III, VI, IX, and XII are outermost and not involved in pore formation.

Correlated Sequence Variations. The quality of a structural model can be assessed by scrutinizing the sequences of homologues. Among homologues, residues which are in direct contact in space but distant in sequence are likely to exhibit either matched conservation or correlated sequence variations that arise due to conservation of molecular volume or matching of polarities (*55*). We have examined the sequences of 51 ProP homologues from prokaryotes (the top 51 matches to full-length sequences from GenBank) for evidence of such correlations at the modeled zones of contact of TM II with TM XI and TM V with TM VIII. These helix pairs form the junction between the N- and C-terminal halves of the MFS structure, and therefore, their interactions are crucial for the conformational changes proposed as the mechanism of transport (*33*). In the TM II−TM XI contact zone, residue 76 (*E. coli* numbering) is F in 48 cases and Y in three cases; these make contact with residue 401 which is always G. Residue 73 is S in 11 cases, always matched by T405. There are 30 cases of A at position 73, and eight of G; these are always matched at position 405 by a larger, nonpolar residue such as L, F, or Y. In the TM V−TM VIII contact zone, I173 contacts M308. In most sequences, I or L contacts M, but there are several instances of either F, W, or Y contacting A, with either A173 opposite Y308 or F173 opposite A308. Thus, conserved residues or correlated residue changes occur at these positions of predicted contact, as expected.

Analysis of ProP Topology and Orientation. Hydropathy analyses of ProP yield both 11- and 12-TM secondary structure models with periplasmic and cytoplasmic N-termini, respectively (*51*). Both MEMSAT (*42*) and our structural model (Figures 1 and 2) suggest that ProP has 12 TMs and cytoplasmic termini. The α-helical segments predicted by our structural model (boxed residues) are more variable in length, and most are longer than the TMs predicted by MEMSAT (groups of bold circles) for two reasons. The membrane-spanning segments in the structural model vary in length (18−25 residues) because some are near normal to the membrane but many are not. (In contrast, hydropathy analyses anticipate a constant length, matching the bilayer normal.) In addition, according to the crystal structures (and hence our structural model), most α-helical segments originate or terminate together at the periplasm but they extend various distances into the cytoplasm. Thus, the length of an α-helical segment often exceeds the length of the corresponding TM (the portion of that α-helical segment within the membrane). We used two methods to test our structural model by assessing the membrane topology and orientation of ProP in vivo.

Analysis of ProP Topology and Orientation of LacZ and PhoA Fusions. In *E. coli*, LacZ is active as *β*-galactosidase only when cytoplasmic and PhoA is active as alkaline phosphatase only when extracytoplasmic. Thus, the enzymatic activities of ProP::LacZ and ProP::PhoA fusion proteins can indicate whether their fusion joints are periplasmic or cytoplasmic (*56*, *57*). Transposons Tn*phoA*/IN and Tn*lacZ*/IN (*58*) were first used in an effort to fuse ′*phoA* and ′*lacZ* to N-terminal *proP*′ fragments. Despite extensive screening, all Tn*lacZ*/IN insertions yielded fusion of ′LacZ to K22 of ProP′ and no active ProP′::′PhoA fusions were recovered. Tn*phoA*/IN and Tn*lacZ*/IN are useful tools for the analysis of membrane topology and the identification of functionally important protein structures (*58*−*60*). However, hot spots for transposon insertion limited the application of this tool to ProP, as to some other proteins (*61*, *62*).

In an alternative approach, full-length fusions of *proP* with ′*phoA* and ′*lacZ* were created by inserting *proP* in vectors pRMCD28 and pRMCD70 (*52*), respectively. Plasmids in which unidirectional deletion of *proP* had created nested *proP*′::′*phoA* or *proP*′::′*lacZ* fusions were prepared as described in Experimental Procedures. The resulting plasmid mixtures were used to transform *E. coli* DH5α (which is devoid of PhoA or LacZ activity under our conditions), and bacteria regaining those activities were identified using indicator media; plasmids were recovered, and fusion joints were identified by restriction analysis and DNA sequencing. This approach yielded an array of independent ′PhoA and ′LacZ fusions (Figure 2).

As expected, in view of the screening process that led to their isolation, the alkaline phosphatase activities of the ′PhoA fusion proteins with fusion joints that mapped in or close to predicted periplasmic loops of ProP (Figure 2) were fairly uniform (mean ± standard deviation of 0.08 ± 0.02 nmol min^{-1} A_{600}^{-1}, Table 2) and more than 1 order of magnitude higher than that of the ProP-E500::PhoA fusion which is shown below to be cytoplasmic. Furthermore, the apparent molecular masses of the fusion proteins decreased in proportion to the lengths of the ProP′ segments (Figure 3). There was not a strong correlation between alkaline phosphatase activity (Table 2) and fusion protein expression level (Figure 3), but some degradation of the fusion proteins was evident. No active ′PhoA fusion was mapped to predicted loop P1 or P3.

The *β*-galactosidase activities of the ′LacZ fusion proteins were much more diverse (range of 0.046−1.178 nmol min^{-1} A_{600}^{-1}) as were the predicted positions of the corresponding fusion joints relative to the membrane (Table 2 and Figure 2). Only a protein with the size of LacZ was detected when anti-LacZ was used to analyze extracts from cells expressing these fusion proteins, and there was no overall correlation between the expression level of this protein and the *β*-galactosidase activity (data not shown). Others have reported analogous results (e.g., refs *62* and *63*) which suggest that the ′LacZ fusion proteins are cleaved near the target protein−

Table 2: Marker Enzyme Activities of Fusion Proteins[a]

marker enzyme	fusion joint	activity	marker enzyme	fusion joint	activity
PhoA	129	79	LacZ	150	270
PhoA	289	85	LacZ	162	296
PhoA	294	61	LacZ	177	197
PhoA	295	63	LacZ	183	135
PhoA	297	93	LacZ	221	228
PhoA	298	95	LacZ	222	274
PhoA	345	73	LacZ	240	314
PhoA	346	68	LacZ	251	313
PhoA	353	113	LacZ	266	74
PhoA	406	69	LacZ	279	57
PhoA	417	42	LacZ	327	448
PhoA	419	127	LacZ	336	253
PhoA	500	0	LacZ	362	46
LacZ	22	784	LacZ	370	400
LacZ	37	1178	LacZ	390	495
LacZ	97	222	LacZ	445	954
LacZ	136	176	LacZ	476	650
LacZ	147	76	LacZ	500	850

[a] Marker enzyme activities of ProP′ fusion proteins (units of 1000 × nanomoles per minute per A_{600}) were determined as described in Experimental Procedures.

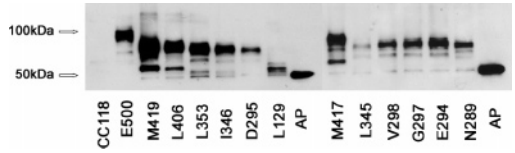

FIGURE 3: Expression levels of ProP′::′PhoA fusion proteins. The expression levels of the ProP′::′PhoA fusion proteins were determined by Western blotting of proteins extracted from the cells prepared for the PhoA assay (Table 2) as described in Experimental Procedures. Electrophoretically separated proteins were transferred to a nitrocellulose membrane, and the fusion proteins were detected with purified anti-alkaline phosphatase. Labels indicate the positions of the fusions (e.g., E500 refers to a PhoA fusion at E500 of ProP). An extract of *E. coli* CC118 (*phoA*$^-$) and *E. coli* alkaline phosphatase (Sigma-Aldrich Corp.) served as a negative and a positive control, respectively (lanes labeled CC118 and AP, respectively). M_r positions at 50 and 100 kDa are indicated.

′LacZ fusion joint and that no further degradation of the ′LacZ fragment occurs. If this occurs prior to membrane insertion, the activity of the resulting fragment will not be a valid indicator of topology for the intact fusion protein.

Most of the active fusions are at positions that were predicted to be on or close to the cytosolic side of the membrane. The fusions at E37, A136, V177, V183, G266, L279, F336, and A362 fall within the membrane according to our structural model (Figure 2), but their activities are consistent with the model after consideration of their location. Half of them (the fusions at E37, V177, G266, and F336) had significant activity but are expected to create hybrid proteins in which the target transmembrane segment would be unable to insert into the membrane once linked to β-galactosidase, a large hydrophilic protein. Rather, the LacZ domain would be expected to remain in the cytoplasm. The others were among the lowest in β-galactosidase activity (0.05−0.18 nmol min^{-1} A_{600}^{-1}).

Analysis of ProP Topology and Orientation by Site-Directed Fluorescence Labeling. Site-directed fluorescence labeling, using fluorescent probe Oregon green maleimide (OGM) coupled with the blocking agent 2-trimethylammonioethyl-methanethiosulfonate (MTSET) (*64*), was used to

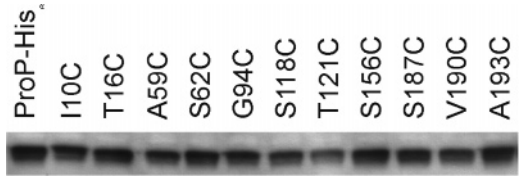

FIGURE 4: Expression levels of ProP variants The expression levels of the ProP* derivatives prepared for this study were compared with that of ProP-His$_6$ by Western blotting as previously described (*51*). The expression levels of the other variants listed in Figure 5 were also similar to that of ProP-His$_6$ as reported elsewhere (*51*; A. P. Hillar, D. E. Culham, Ya. I. Vernikovska, J. M. Wood, and J. M. Boggs, unpublished data).

complement the data described above. This analysis focused primarily on the N-terminal half of ProP since no ′PhoA fusions had been recovered in or near predicted loop P1 or P3. In addition, ′LacZ and ′PhoA fusion analyses are not definitive if the incorporated, N-terminal fragment of the target protein is too short (*61*). The target residues included the four native Cys residues of ProP (C112, C133, C264, and C367) and the Cys that replaced other native residues in the periplasmic or cytoplasmic loops or termini predicted by our structural model (see Figure 1B and native or introduced Cys, colored yellow, in Figure 2). All were expressed in the background of our fully functional, Cys-less ProP variant, ProP*. Both OGM and MTSET are membrane impermeant reagents that react with cysteine thiols, but only OGM is fluorescent. OGM labels Cys residues exposed to the periplasm of intact cells, but it labels those exposed to the cytoplasm only after cell lysis. If intact cells are treated with MTSET before membrane preparation by cell lysis, subsequent treatment with OGM labels only Cys residues exposed on the cytoplasmic surface of the membrane. We previously used this approach to demonstrate that C293 of ProP* is periplasmic and C241 of ProP* is cytoplasmic (*51*).

The expression levels, activities, and osmotic activation thresholds of the single Cys variants were assessed (Figures 4 and 5). Most were expressed at a level similar to that of ProP-His$_6$ (the level of expression of ProP*-T121C was reduced approximately 2-fold) [Figure 4 (*51*)]. With the exception of ProP*-G94C, all variants exhibited sufficient activity to serve as reliable targets for fluorescence labeling (Figure 5, middle left). Intact *E. coli* cells and permeabilized membranes prepared from MTSET-blocked and unblocked cells were treated with OGM; the ProP* variants were purified, and their fluorescence was expressed per unit of ProP protein (Figure 5, top left; representative primary data are shown in Figure 6). In most cases, residues predicted to be periplasmic (green) were labeled in intact bacteria much more than in membranes from MTSET-blocked cells, whereas the converse was true of residues that were predicted to be cytoplasmic (pink). Residues predicted to be cytoplasmic were labeled to similar extents in membranes from unblocked and MTSET-blocked cells (for an example, see Figure 6).

Each native Cys (blue) was predicted to reside within a TM (Figure 2). Residues 112, 133, and 264 were poorly labeled as expected on this basis and reported before (*51*). The positions of these residues are illustrated on our structural model for ProP in Figure 5 (right). Although C264 appears to be near the cytoplasmic end of TM VII and exposed, the

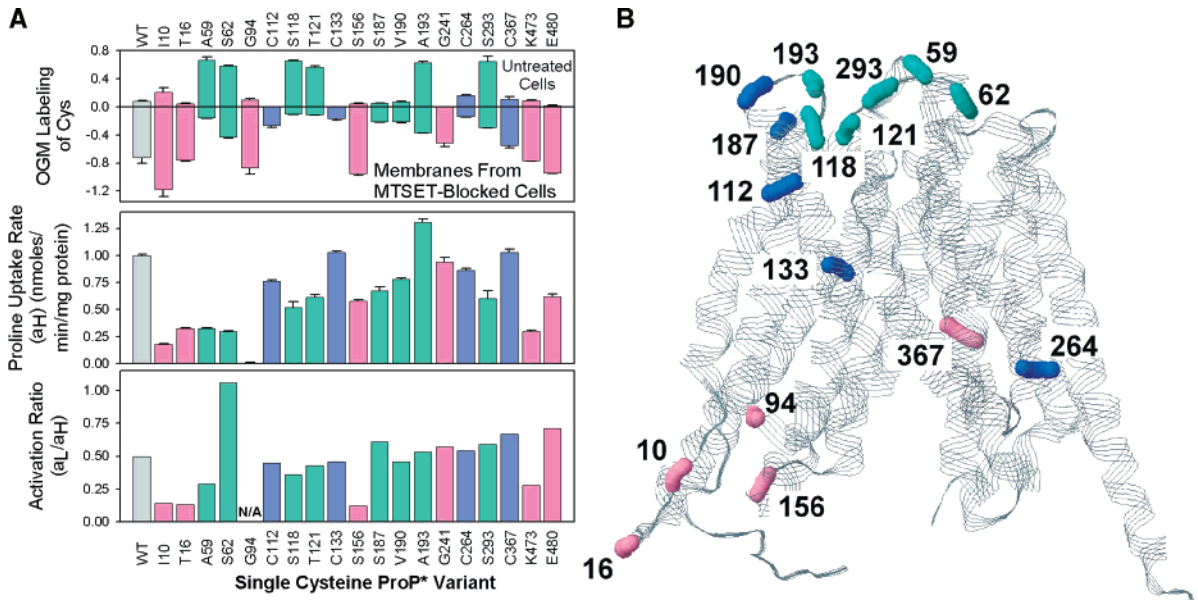

FIGURE 5: Characterization of ProP variants and analysis of ProP topology and orientation by site-directed fluorescence labeling. (A) Plasmids encoding ProP* derivatives with the indicated Cys replacements were created, and the proline uptake activities of bacteria expressing those derivatives were determined as described in Experimental Procedures. For transport assays, bacteria were cultivated in NaCl-free MOPS medium and assay media were supplemented with NaCl at 50 mM (a_L) or 170 mM (a_H). The expression levels of these ProP variants are illustrated in Figure 4. OGM labeling of the Cys in each variant was assessed as the ratio of densities of fluorescent and Coomassie Blue-stained bands in intact cells (positive values) or in membrane vesicles after blocking residues exposed in the intact cells with MTSET (negative values) to probe their periplasmic and cytoplasmic exposure, respectively (see Figure 6). The mean of duplicate gels, each run in triplicate, ± the range is shown. Gray bars are data for ProP-His_6, which retains all four native Cys residues. Pink, blue, and green bars are data for Cys residues that are predicted to be cytoplasmic, within transmembrane domains, and periplasmic, respectively, according to the structural model in Figures 1B and 2. (B) The positions of the ProP residues replaced with Cys and treated with OGM are shown on the structural model of ProP (Figure 2). Residues colored pink and green were labeled best in intact bacteria and permeabilized membranes from MTSET-blocked cells, respectively, whereas residues colored blue were not labeled well in either preparation (see panel A and Figure 7). The failure of residues C187 and C190 to be labeled with OGM and the labeling of C367 in permeabilized membranes were unexpected (compare panels A and B; see the text for a discussion).

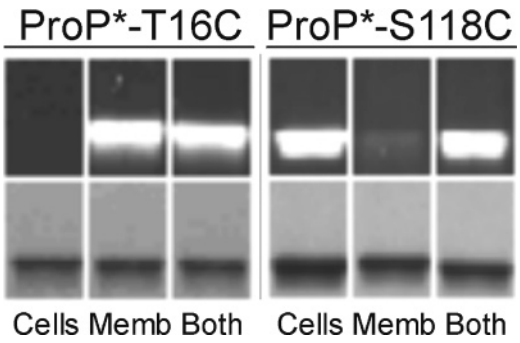

FIGURE 6: OGM labeling of Cys in variants ProP*-T16C and ProP*-S118C. OGM labeling, MTSET blocking, recovery of labeled protein by Ni−NTA chromatography, SDS−PAGE, and visualization of the resulting gels were conducted as described in Experimental Procedures. The top panels show fluorescence and the bottom panels Coomassie Blue staining of the same SDS−PAGE gels. Intact cells were labeled externally with OGM (Cells); cells were blocked with MTSET and lysed, and permeabilized membranes were labeled with OGM (Memb) or membranes from unblocked cells labeled with OGM (Both). Figure 5A shows the fluorescence-to-protein ratios (mean ± range) determined by densitometry from a typical experiment in which duplicate gels were used to analyze triplicate samples.

model reveals that C264 is enclosed in the bundle formed by helices VII and X−XII which extends well into the cytpoplasm, and is not solvent-exposed. In contrast, residue C367 was well labeled in membranes from MTSET-blocked cells and thus appeared to have significant cytoplasmic exposure (Figure 5). Despite being deeper within the membrane than C264, our structural model suggests that this side chain may be accessible in the central cleft of the transporter in its inward-facing conformation. C367 is partly covered only by the ends of TMs VIII and IX, which do not project far into the cytoplasm, and which may be relatively mobile as the transporter switches conformations.

Exposure of Residues in Predicted Loop P3. The existence of loop P3 was confirmed by good OGM labeling of residue C193 in intact bacteria. Nearby residues C187 and C190 were labeled poorly in both intact bacteria and isolated, permeabilized membranes (Figure 5), but they were labeled well after SDS solubilization and denaturation of ProP. (The degree of labeling of C187 in this context was approximately 60% of that of other residues, including C190, C241, and C293.) The accessibility of those residues was further probed by treating intact cells or permeabilized membranes with various methanethiosulfonate (MTS) reagents, isolating the corresponding ProP* variants, denaturing with SDS, and then labeling them with OGM. These data were expressed as percent blockage of the OGM labeling of the unblocked, SDS-treated ProP* variant (Figure 7). The blocking reagents applied to the intact cells or membranes included MTSET (cationic), MTSEA (2-aminoethyl-methanethiosulfonate, a mixture of positively charged and uncharged species at pH 8, as used for labeling), and MTSES (2-sulfonatoethyl-methanethiosulfonate, anionic). MTSET, MTSES, and cationic MTSEA are membrane impermeant, whereas uncharged MTSEA is membrane permeant (*65*).

Significant blockage of OGM labeling by pretreatment of intact cells with membrane impermeant reagent MTSET

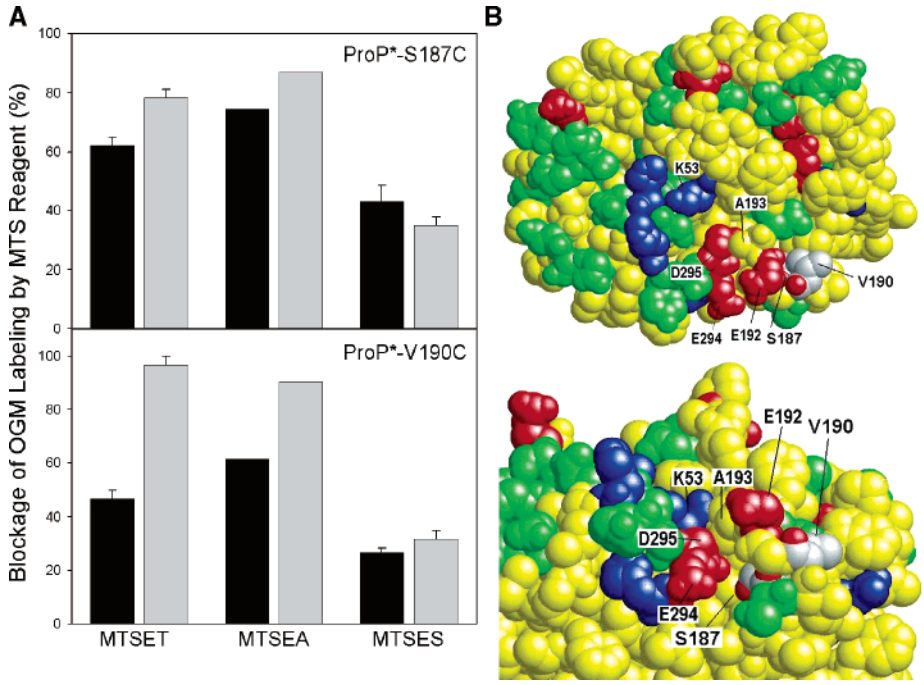

FIGURE 7: MTS reagents differentially block OGM labeling of C187 and C190. (A) OGM labeling was conducted as described in Experimental Procedures and the legend of Figure 6, with the exception that purified ProP was labeled with OGM in SDS after treatment of cells or membranes with an MTS reagent (MTSET, MTSEA, or MTSES). The graph shows the percent blockage of OGM labeling by MTS reagent for cells (black bars) and membranes (gray bars) relative to unblocked labeling in SDS. (B) Location of S187 and V190 (both gray) in the ProP model. These residues are partly buried and adjacent to acidic side chains (red; see the text for further discussion): (top) ProP viewed from the periplasm and (bottom) view of the periplasmic surface of ProP from the membrane plane.

indicated that residues C187 and C190 are periplasmic, as predicted (Figure 2). However, even greater blockage occurred, particularly for residue C190, when membranes were isolated before treatment with MTSET or MTSEA, followed by OGM labeling in SDS. It is unlikely that the structure of ProP is seriously disrupted during membrane preparation since it remains active as an osmosensor and transporter in cytoplasmic membrane vesicles (*18*). Alternative explanations for these results are provided below (see the Discussion).

When applied to intact cells, anionic reagents MTSES and OGM reacted with these residues much less efficiently than MTSET and MTSEA which are both cationic (or uncharged, in the case of MTSEA). This suggests that these residues are at sites of protein−protein or protein−phospholipid headgroup interaction, where local charged residues influence reagent accessibility. Both S187 and V190 are near the surface of the protein adjacent to the phospholipid bilayer (Figure 5, right) and near the side chains of acidic residues. Our model shows a cluster of three anionic residues, E192, E294, and D295 (shown in red in Figure 7B), which lie close to the loop containing S187 and V190. Electrostatic fields calculated by SPDBV indicated that V190 lies in the negative field of E192, but that the presence of K53 moderates the negative field in the region of A193, allowing for effective labeling of Cys at that position.

Exposure of Residues S62 and A193. In comparison to residues that were labeled in cells but not in permeabilized membranes from MTSET-blocked cells (e.g., C118), residues C62 and C193 exhibited significant labeling in both preparations (Figure 5). Therefore, the effect of blocking these residues with MTS reagents of different charge or permeability, MTSEA and MTSES, was also determined, and their labeling by OGM was expressed relative to their labeling in permeabilized, membrane preparations from unblocked cells.

The labeling of residues C62 and C193 in intact cells was a smaller fraction of their labeling in permeabilized membranes from unblocked cells than was true for other periplasmic residues (shown for C118 in Figure 8, top left panel). Residues C62 and C193 were also labeled to a significant extent in permeabilized membranes from cells blocked with membrane impermeant reagent MTSET or MTSES (Figure 8, top right panel, black and dark gray bars, respectively), though that labeling was effectively blocked by permeant reagent MTSEA (Figure 8, top right, light gray bars). This apparent labeling of C62 and C193 from both membrane surfaces is analogous to that discussed above for residues C187 and C190. Its origin is discussed further below (see the Discussion).

Impacts of Cys Substitutions on the Activity and Osmotic Activation of ProP.* As noted above, each of the ProP* variants prepared for this study was characterized to determine the impact of each Cys substitution on the activity and osmotic activation of ProP (Figure 5A). Notably, the variants with Cys replacements predicted to reside in the cytoplasmic N-terminus (I10C and T16C) or putative periplasmic loop 1 (P1 of Figure 2, A59C and S62C) were lower in activity than ProP*, while variant ProP*-G94C, with Cys predicted to reside in cytoplasmic loop 1 (loop C1 of Figure 2), was devoid of activity. Furthermore, the variants with replacements I10C, T16C, A59C, and S156C had low activation ratios (Figure 5A, bottom panel), suggesting that their thresholds for osmotic activation had been elevated (*51*). In contrast, the activation ratio increased (and hence the osmotic activation threshold appeared to be diminished) for variant ProP*-S62C. In fact, the activities of both ProP*-S62C (not

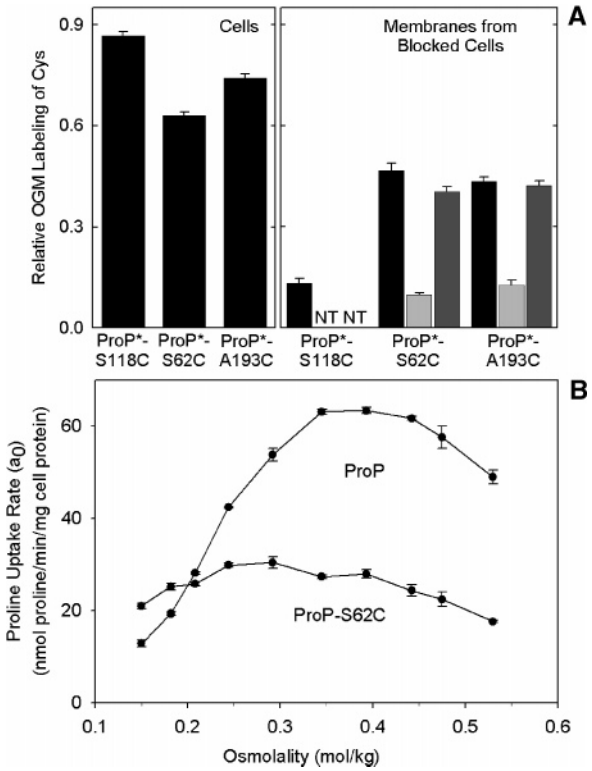

FIGURE 8: Surface exposure and functional effects of C62 and C193. (A) MTS reagents differentially block OGM labeling of C62 and C193. OGM labeling was as described in Experimental Procedures and the legend of Figure 6 except that here we report the ratio of labeling of ProP in intact cells or in membranes after blocking cells to that in membranes from unblocked cells (total labeling from both sides). The left and right panels show the unblocked labeling of cells and the labeling of membranes after blocking in cells, respectively. Blocking of residues exposed in intact cells was performed with MTSET (black bars), MTSEA (light gray bars), or MTSES (dark gray bars). (B) Replacement S62C renders ProP refractory to osmotic activation. The initial rate of proline uptake via ProP-S62C was measured as a function of osmolality in NaCl-supplemented MOPS media as described in Experimental Procedures. The activity of ProP, determined under the same conditions, is also shown for comparison (data derived from Figure 2 of ref *51*).

shown) and ProP-S62C (Figure 8B) were essentially independent of osmolality over a broad range. This is the first evidence that residues close to the N-terminus are critical for the activity and the osmotic activation of ProP, and ProP-S62C is the first constitutively active ProP variant to be isolated.

DISCUSSION

Structural Model for ProP. In the past, the transmembrane topologies of MFS transporters such as ProP could only be predicted by applying principles derived from known structures for other classes of integral membrane proteins (*66*). It has now become possible to model ProP and other MFS proteins by aligning them with LacY and GlpT (Figure 1S of the Supporting Information). Our structural model (Figure 1B) and most hydropathy analyses (*51*) predict similar overall membrane topologies and orientations for ProP (compared in Figure 2), but some TMs differ in position from those predicted by hydropathy analysis.

Two experimental approaches were used to begin testing these models. ProP′::′LacZ and ProP′::′PhoA fusion proteins with marker enzyme activity were created and their fusion joints located to define regions of ProP that were cytoplasmic and periplasmic, respectively (Figure 2). Fusion analysis cannot reliably define the topology and orientation of TMs near a target protein's N-terminus because the membrane topologies of fusion proteins may be influenced by the absence of target protein residues that normally occur beyond the fusion joint (*61*). Fusion-derived data were therefore supplemented with site-directed fluorescence labeling, primarily focusing on residues within the N-terminal half of ProP (Figures 2 and 5). Site-directed labeling depends on the local environment of each introduced Cys residue as well as on the position of that residue relative to the permeability barrier of the cytoplasmic membrane. Thus, detailed experimentation was required to determine the topology of some target residues (e.g., Figures 7 and 8). Since both approaches were applied to intact bacteria, both defined the in vivo topology and orientation of ProP.

The overall topology and orientation of ProP illustrated in Figures 1 and 2 are supported by the data presented in Figures 2−6. At least one ′PhoA fusion junction or at least one Cys residue labeled with OGM (and/or blocked by MTSET) in intact bacteria is found in or adjacent to each putative periplasmic loop. Likewise, at least one ′LacZ fusion junction or at least one Cys residue labeled with OGM only in permeabilized membranes from MTSET-blocked cells is found in the N-terminus, in or near each putative cytoplasmic loop and the C-terminus of the protein. These data are also consistent with ′PhoA fusion analysis of the closely related *E. coli* protein KgtP (*67*).

Transport Mechanism of ProP. ProP is a H^+-osmoprotectant symporter; LacY is a H^+-β-galactoside symporter, and GlpT is an organic anion antiporter. All are believed to function via the alternating access model of transport in which one (GlpT) or two (LacY and ProP) substrates bind to an outward (periplasm)-facing conformation of the transporter, the N- and C-terminal six-helix bundles tilt around an axis in the plane of the membrane to form the inward (cytoplasmic)-facing conformation, and one or two substrates are released to the cytoplasm. For GlpT, a substrate binds from the cytoplasmic surface before the transporter returns to its outward-facing conformation and the substrate is released to the periplasm. For LacY and ProP, the transporter returns to its outward-facing conformation in the unloaded state (*68*). Given their different applications of the alternating access model, significant differences between the GlpT and LacY structures [such that their superimposition gives an rms deviation of 2.46 Å (*69*)] are not surprising. Although the ProP sequence can be modeled to the GlpT template easily, the true structure of ProP may deviate from the structures of GlpT and LacY by as much as they deviate from each other.

Speculation about substrate binding sites or details of the transport mechanism for ProP based on this model would be premature. Nevertheless, one readily testable prediction may be made. Ionizable residues implicated in proton translocation and coupling to lactose transport fall within a pathway formed by transmembrane helices VII−X, in the C-terminal half of LacY (*33*). According to our structural model (Figure 1B), the C-terminal half of ProP lacks internally oriented, charged residues that might make up such a pathway. Instead, the N-terminal half of ProP contains

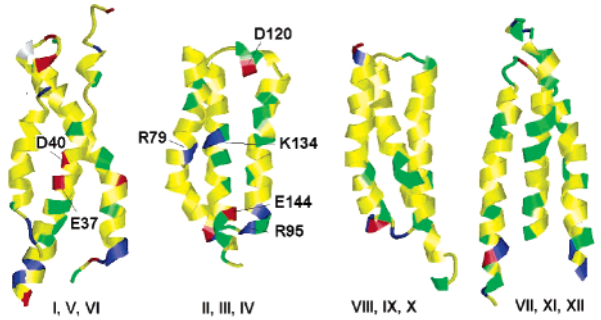

FIGURE 9: ProP model viewed from the inside of the substrate channel. The structure is divided into the four braided clusters. The side facing the viewer is buried in the core of the protein. Several charged side chains within TMs I−VI face the interior and may contribute to a proton-conducting channel. In contrast, TMs VII−XII contain a few polar residues, but no charged amino acids other than those exposed at the cytoplasmic and periplasmic faces: yellow for nonpolar, green for polar and uncharged, blue for positive, and red for negative.

several ionizable amino acids that may contribute to passage of H^+ (Figure 9).

Among the conservative Cys substitutions introduced into ProP* for labeling during this study, G94C was the only one that abrogated transport activity (Figure 5A, middle panel). Dipeptide G94-R95 falls within the [RK]-x-x-[RK]-[RK] motif (K92-Y93-G94-R95-Q96-K97) and constitutes the short link between transmembrane helices II and III. This motif is found in loops C1 and C4 of all MFS members. ProP*-G94C was incorporated into the membrane and labeled with OGM only in permeabilized membrane preparations (Figure 5), and an active LacZ fusion occurred at residue K97 (Figure 2). These observations substantiate the existence of loop C1 and conformity of ProP to shared features of the alternating access model. Since mutations within this motif impair function for many systems, it may be involved in maintaining the curvature of and facilitating conformational changes involving these helices (*68*).

Osmosensing and the Osmoregulation of ProP Activity. ProP, BetP, and OpuA are osmosensors because chemically diverse, membrane impermeant osmolytes have quantitatively similar effects on their activities when used to adjust cell or proteoliposome suspensions to the same osmolality. In contrast, the activity of each system depends on the composition of the lumenal solvent in proteoliposomes (*16*). The in vitro responses of all three systems to lumenal electrolytes suggest models for osmosensing based on electrostatic interactions or ion binding (*16*, *70*). The ProP response to lumenal macromolecules suggests a model based on changes in hydration or macromolecular crowding (*16*). These transporters could possess cytoplasmic regulatory domains whose interactions would be modulated by cytoplasmic ionic strength and/or macromolecular crowding to determine transporter activity (*16*, *70*). ProP does possess a distinct, cytoplasmic domain (the coiled coil formed by adjacent ProP C-termini), but it appears to modulate the threshold for osmotic activation rather than acting as an osmosensor, per se (*36*; Y. Tsatskis and J. M. Wood, unpublished data).

We therefore seek evidence that additional structural elements are involved in osmosensing by ProP, bearing in mind that similar osmolality changes activate ProP and inhibit respiration and the activities of transporters that are not osmosensors, including LacY (*3*). Ultimately, osmolality changes must modulate proton-osmoprotectant symport by changing structures involved in the alternating access mechanism. Osmosensing and osmoregulation of ProP activity could be combined if osmolality changes altered the packing of the N- and C-terminal helix bundles and/or the occurrence and positioning of key water molecules within the ion and/or substrate translocation pathways. It is interesting that, in this study, replacement of residues at the ends of the putative H^+ pathway through the N-terminal helix bundle of ProP significantly perturbed its osmotic activation (cytoplasmic residues I10, I16, and S156 and periplasmic residues A59, S62, and A193; Figure 5).

Despite clear evidence that they are exposed to the periplasm, some residues reacted to a greater extent with labeling and/or blocking reagents in permeabilized membrane preparations than in intact cells [C62 (loop P1), C187, C190, and C193 (loop P3)] (Figures 5, 7 and 8). For other proteins, such data are believed to indicate accessibility of such residues to membrane impermeant reagents from both the cytoplasmic and periplasmic membrane surfaces in preparations that may include mixtures of transporters with outward- and inward-facing conformations. The residues in question are near the membrane in the inward-facing conformation portrayed by our model (Figures 5 and 7B). C187 and C190 were accessible only to neutral and positively charged reagents, not to negatively charged OGM and MTSES, supporting the model in which they are partly buried and adjacent to acidic side chains (Figure 7B). Cytoplasmic, rather than periplasmic, exposure of these residues is inconsistent with this model, and it appears unlikely that these residues would be exposed to the cytoplasm when ProP assumes other conformations during the transport cycle.

Alternatively, membrane preparation may increase the level of exposure of residues on the periplasmic surface of ProP because that exposure depends on osmolality-dependent properties of the cytoplasm, such as its ion composition, ionic strength, and macromolecular crowding, that are lost during membrane preparation. If so, modulation of medium osmolality may be expected to modulate the covalent modification of periplasmic residues in intact bacteria. The facts that osmosensing is perturbed by replacement of residues on the periplasmic surface of ProP (including A59 and S62, Figure 5) and that membrane preparation enhances covalent labeling of C187, C190, and C193 (Figures 7 and 8) are consistent with these concepts.

ACKNOWLEDGMENT

We are grateful to Colin Manoil and Beth Traxler for Tn*lacZ*/IN and Tn*phoA*/IN, to David Wan, Monica Pearson, Petra Bochtler, and Craig Campbell for their work with those systems as probes for the membrane topology and orientation of ProP, and to Craig Daniels for plasmids pRMCD28 and pRMCD70.

SUPPORTING INFORMATION AVAILABLE

Multiple-sequence alignment of ShiA, ProP, KgtP, LacY, and GlpT (Figure 1S) and structure-based alignment of ProP onto GlpT (1PW4) (Figure 2S). This material is available free of charge via the Internet at http://pubs.acs.org.

REFERENCES

1. Roesser, M., and Muller, V. (2001) Osmoadaptation in bacteria and archaea: Common principles and differences, *Environ. Microbiol. 3*, 743−754.
2. Roberts, M. F. (2000) Osmoadaptation and osmoregulation in archaea, *Front. Biosci. 5*, D796−D812.
3. Wood, J. M. (1999) Osmosensing by Bacteria: Signals and Membrane-Based Sensors, *Microbiol. Mol. Biol. Rev. 63*, 230−262.
4. Martinac, B. (2001) Mechanosensitive channels in prokaryotes, *Cell. Physiol. Biochem. 11*, 61−76.
5. Stein, W. D. (2002) Cell volume homeostasis: Ionic and nonionic mechanisms. The sodium pump in the emergence of animal cells, *Int. Rev. Cytol. 215*, 231−258.
6. Hohmann, S. (2002) Osmotic adaptation in yeast: Control of the yeast osmolyte system, *Int. Rev. Cytol. 215*, 149−187.
7. Sardini, A., Amey, J. S., Weylandt, K. H., Nobles, M., Valverde, M. A., and Higgins, C. F. (2003) Cell volume regulation and swelling-activated chloride channels, *Biochim. Biophys. Acta 1618*, 153−162.
8. Burg, M. B. (2002) Response of renal inner medullary epithelial cells to osmotic stress, *Comp. Biochem. Physiol., Part A: Mol. Integr. Physiol. 133*, 661−666.
9. Barbier-Brygoo, H., Vinauger, M., Colcombet, J., Ephritikhine, G., Frachisse, J., and Maurel, C. (2000) Anion channels in higher plants: Functional characterization, molecular structure and physiological role, *Biochim. Biophys. Acta 1465*, 199−218.
10. Rontein, D., Basset, G., and Hanson, A. D. (2002) Metabolic engineering of osmoprotectant accumulation in plants, *Metab. Eng. 4*, 49−56.
11. Racher, K. I., Voegele, R. T., Marshall, E. V., Culham, D. E., Wood, J. M., Jung, H., Bacon, M., Cairns, M. T., Ferguson, S. M., Liang, W.-J., Henderson, P. J. F., White, G., and Hallett, F. R. (1999) Purification and reconstitution of an osmosensor: Transporter ProP of *Escherichia coli* senses and responds to osmotic shifts, *Biochemistry 38*, 1676−1684.
12. Rübenhagen, R., Roensch, H., Jung, H., Krämer, R., and Morbach, S. (2000) Osmosensor and osmoregulator properties of the betaine carrier BetP from *Corynebacterium glutamicum* in proteoliposomes, *J. Biol. Chem. 275*, 735−741.
13. van der Heide, T., and Poolman, B. (2000) Osmoregulated ABC-transport system of *Lactococcus lactis* senses water stress via changes in the physical state of the membrane, *Proc. Natl. Acad. Sci. U.S.A. 97*, 7102−7106.
14. Morbach, S., and Krämer, R. (2002) Body shaping under water stress: Osmosensing and osmoregulation of solute transport in bacteria, *ChemBioChem 3*, 384−397.
15. Poolman, B., Blount, P., Folgering, J. H. A., Friesen, R. H. E., Moe, P. C., and van der Heide, T. (2002) How do membrane proteins sense water stress? *Mol. Microbiol. 44*, 889−902.
16. Poolman, B., Spitzer, J. J., and Wood, J. M. (2004) Bacterial Osmosensing: Roles of membrane structure and electrostatics in lipid−protein and protein−protein interactions, *Biochim. Biophys. Acta 1666*, 88−104.
17. Culham, D. E., Lasby, B., Marangoni, A. G., Milner, J. L., Steer, B. A., van Nues, R. W., and Wood, J. M. (1993) Isolation and sequencing of *Escherichia coli* gene *proP* reveals unusual structural features of the osmoregulatory proline/betaine transporter, ProP, *J. Mol. Biol. 229*, 268−276.
18. Milner, J. L., Grothe, S., and Wood, J. M. (1988) Proline porter II is activated by a hyperosmotic shift in both whole cells and membrane vesicles of *Escherichia coli* K12, *J. Biol. Chem. 263*, 14900−14905.
19. MacMillan, S. V., Alexander, D. A., Culham, D. E., Kunte, H. J., Marshall, E. V., Rochon, D., and Wood, J. M. (1999) The ion coupling and organic substrate specificities of osmoregulatory transporter ProP in *Escherichia coli*, *Biochim. Biophys. Acta 1420*, 30−44.
20. Racher, K. I., Culham, D. E., and Wood, J. M. (2001) Requirements for osmosensing and osmotic activation of transporter ProP from *Escherichia coli*, *Biochemistry 40*, 7324−7333.
21. Culham, D. E., Henderson, J., Crane, R. A., and Wood, J. M. (2003) Osmosensor ProP of *Escherichia coli* responds to the concentration, chemistry and molecular size of osmolytes in the proteoliposome lumen, *Biochemistry 42*, 410−420.
22. Rübenhagen, R., Morbach, S., and Krämer, R. (2001) The osmoreactive betaine carrier BetP from *Corynebacterium glutamicum* is a sensor for cytoplasmic K^+, *EMBO J. 20*, 5412−5420.
23. Schiller, D., Rübenhagen, R., Krämer, R., and Morbach, S. (2004) The C-terminal domain of the betaine carrier BetP of *Corynebacterium glutamicum* is directly involved in sensing K^+ as an osmotic stimulus, *Biochemistry 43*, 5583−5591.
24. Schiller, D., Krämer, R., and Morbach, S. (2004) Cation specificity of osmosensing by the betaine carrier BetP of *Corynebacterium glutamicum*, *FEBS Lett. 563*, 108−112.
25. Milner, J. L., and Wood, J. M. (1989) Insertion *proQ220*::Tn*5* alters regulation of proline porter II, a transporter of proline and glycine betaine in *Escherichia coli*, *J. Bacteriol. 171*, 947−951.
26. Kunte, H. J., Crane, R. A., Culham, D. E., Richmond, D., and Wood, J. M. (1999) Protein ProQ influences osmotic activation of compatible solute transporter ProP in *Escherichia coli* K-12, *J. Bacteriol. 181*, 1537−1543.
27. Smith, M. N., Crane, R. A., Keates, R. A. B., and Wood, J. M. (2004) Overexpression, purification and characterization of ProQ, a post-translational regulator for osmoregulatory transporter ProP of *Escherichia coli*, *Biochemistry 43*, 12979−12989.
28. Privé, G. G., and Kaback, H. R. (1996) Engineering the Lac permease for purification and crystallization, *J. Bioenerg. Biomembr. 28*, 29−34.
29. Ward, A., O'Reilly, J., Rutherford, N. G., Ferguson, S. M., Hoyle, C. K., Palmer, S. L., Clough, J. L., Venter, H., Xie, H., Litherland, G. J., Martin, G. E., Wood, J. M., Roberts, P. E., Groves, M. A., Liang, W. J., Steel, A., McKeown, B. J., and Henderson, P. J. (1999) Expression of prokaryotic membrane transport proteins in *Escherichia coli*, *Biochem. Soc. Trans. 27*, 893−899.
30. Saidijam, M., Psakis, G., Clough, J. L., Meuller, J., Suzuki, S., Hoyle, C. J., Palmer, S. L., Morrison, S. M., Pos, M. K., Essenberg, R. C., Maiden, M. C., Abu-bakr, A., Baumberg, S. G., Neyfakh, A. A., Griffith, J. K., Stark, M. J., Ward, A., O'Reilly, J., Rutherford, N. G., Phillips-Jones, M. K., and Henderson, P. J. (2003) Collection and characterisation of bacterial membrane proteins, *FEBS Lett. 555*, 170−175.
31. Hirai, T., Heymann, J. A., Shi, D., Sarkar, R., Maloney, P. C., and Subramaniam, S. (2002) Three-dimensional structure of a bacterial oxalate transporter, *Nat. Struct. Biol. 9*, 597−600.
32. Huang, Y., Lemieux, M. J., Song, J., Auer, M., and Wang, D.-N. (2003) Structure and mechanism of the glycerol-3-phosphate transporter from *Escherichia coli*, *Science 301*, 616−620.
33. Abramson, J., Smirnova, I., Kasho, V., Verner, G., Kaback, H. R., and Iwata, S. (2003) Structure and mechanism of the lactose permease of *Escherichia coli*, *Science 301*, 610−615.
34. Hirai, T., Heymann, J. A. W., Maloney, P. C., and Subramaniam, S. (2003) Structural model for 12-helix transporters belonging to the major facilitator superfamily, *J. Bacteriol. 185*, 1712−1718.
35. Kaback, H. R., Sahin-Toth, M., and Weinglass, A. B. (2001) The kamikaze approach to membrane transport, *Nat. Rev. Mol. Cell Biol. 2*, 610−620.
36. Culham, D. E., Tripet, B., Racher, K. I., Voegele, R. T., Hodges, R. S., and Wood, J. M. (2000) The role of the carboxyl terminal α-helical coiled-coil domain in osmosensing by transporter ProP of *Escherichia coli*, *J. Mol. Recognit. 13*, 1−14.
37. Zoetewey, D. L., Tripet, B. P., Kutateladze, T. G., Overduin, M. J., Wood, J. M., and Hodges, R. S. (2003) Solution structure of the C-terminal antiparallel coiled-coil domain from *Escherichia coli* osmosensor ProP, *J. Mol. Biol. 334*, 1063−1076.
38. Hillar, A., Tripet, B., Zoetewey, D., Wood, J. M., Hodges, R. S., and Boggs, J. M. (2003) Detection of α-helical coiled-coil dimer formation by spin-labeled synthetic peptides: A model parallel coiled-coil peptide and the antiparallel coiled-coil formed by a replica of the ProP C-terminus, *Biochemistry 42*, 15170−15178.
39. Peter, H., Burkovski, A., and Krämer, R. (1998) Osmo-sensing by N- and C-terminal extensions of the glycine betaine uptake system BetP of *Corynebacterium glutamicum*, *J. Biol. Chem. 273*, 2567−2574.
40. Jones, D. T. (1999) Protein secondary structure prediction based on position-specific scoring matrices, *J. Mol. Biol. 292*, 195−202.
41. Cuff, J. A., Clamp, M. E., Siddiqui, A. S., Finlay, M., and Barton, G. J. (1998) JPred: A consensus secondary structure prediction server, *Bioinformatics 14*, 892−893.
42. Jones, D. T., Taylor, W. R., and Thornton, J. M. (1994) A model recognition approach to the prediction of all-helical membrane protein structure and topology, *Biochemistry 33*, 3038−3049.
43. Thompson, J. D., Higgins, D. G., and Gibson, T. J. (1994) CLUSTAL W: Improving the sensitivity of progressive multiple

sequence alignment through sequence weighting, position-specific gap penalties and weight matrix choice, *Nucleic Acids Res. 22*, 4673−4680.
44. Guex, N., and Peitsch, M. C. (1997) SWISS-MODEL and the Swiss-PdbViewer: An environment for comparative protein modeling, *Electrophoresis 18*, 2714−2723.
45. Kelley, L. A., MacCallum, R. M., and Sternberg, M. J. E. (2000) Enhanced Genome Annotation using Structural Profiles in the Program 3D-PSSM, *J. Mol. Biol. 299*, 499−520.
46. Miller, J. H. (1972) *Experiments in Molecular Genetics*, Cold Spring Harbor Laboratory Press, Plainview, NY.
47. Neidhardt, F. C., Bloch, P. L., and Smith, D. F. (1974) Culture medium for enterobacteria, *J. Bacteriol. 119*, 736−747.
48. Sambrook, J., Frisch, E. F., and Maniatis, T. (1989) *Molecular Cloning: A Laboratory Manual*, 2nd ed., Cold Spring Harbor Laboratory Press, Plainview, NY.
49. Brown, E. D., and Wood, J. M. (1992) Redesigned purification yields a fully functional PutA protein dimer from *Escherichia coli*, *J. Biol. Chem. 267*, 13086−13092.
50. Guzman, L.-M., Belin, D., Carson, M. J., and Beckwith, J. (1995) Tight regulation, modulation, and high-level expression by vectors containing the arabinose P_{BAD} promoter, *J. Bacteriol. 177*, 4121−4130.
51. Culham, D. E., Hillar, A., Henderson, J., Ly, A., Vernikovska, Ya. I., Racher, K. I., Boggs, J. M., and Wood, J. M. (2003) Creation of a fully functional, cysteine-less variant of osmosensor and proton-osmoprotectant symporter ProP from *Escherichia coli* and its application to assess the transporter's membrane orientation, *Biochemistry 42*, 11815−11823.
52. Daniels, C., Vindurampulle, C., and Morona, R. (1998) Overexpression and topology of the *Shigella flexneri* O-antigen polymerase (Rfc/Wzy), *Mol. Microbiol. 28*, 1211−1222.
53. Hanahan, D. (1983) Studies on transformation of *Escherichia coli* with plasmids, *J. Mol. Biol. 166*, 557−569.
54. Zuniga, F. A., Shi, G., Haller, J. F., Rubashkin, A., Flynn, D. R., Iserovich, P., and Fischbarg, J. (2001) A three-dimensional model of the human facilitative glucose transporter Glut1, *J. Biol. Chem. 276*, 44970−44975.
55. Olmea, O., and Valencia, A. (1997) Improving contact predictions by the combination of correlated mutations and other sources of sequence information, *Folding Des. 2*, S25−S32.
56. Manoil, C. (1991) Analysis of membrane protein topology using alkaline phosphatase and β-galactosidase gene fusions, *Methods Cell Biol. 34*, 61−75.
57. Manoil, C. (1990) Analysis of protein localization by use of gene fusions with complementary properties, *J. Bacteriol. 172*, 1035−1042.
58. Manoil, C., and Bailey, J. (1997) A simple screen for permissive sites in proteins: Analysis of *Escherichia coli lac* permease, *J. Mol. Biol. 267*, 250−263.
59. Hayes, F. (2003) Transposon-based strategies for microbial functional genomics and proteomics, *Annu. Rev. Genet. 37*, 3−29.
60. Bailey, J., and Manoil, C. (2002) Genome-wide internal tagging of bacterial exported proteins, *Nat. Biotechnol. 20*, 839−842.
61. Hu, L. A., and King, S. C. (1998) Membrane topology of the *Escherichia coli* γ-aminobutyrate transporter: Implications on the topography and mechanism of prokaryotic and eukaryotic transporters from the APC superfamily, *Biochem. J. 336*, 69−76.
62. Thomas, G. H., Mullins, J. G. L., and Merrick, M. (2000) Membrane topology of the Mep/Amt family of ammonium transporters, *Mol. Microbiol. 37*, 331−344.
63. Gandlur, S. M., Wei, L., Levine, J., Russell, J., and Kaur, P. (2004) Membrane topology of the DrrB protein of the doxorubicin transporter of *Streptomyces peucetius*, *J. Biol. Chem. 279*, 27799−27806.
64. Ye, L., Jia, Z., Jung, T., and Maloney, P. C. (2001) Topology of OxlT, the oxalate transporter of *O. formigenes*, determined by site-directed fluorescence labeling, *J. Bacteriol. 183*, 2490−2496.
65. Holmgren, M., Liu, Y., Xu, Y., and Yellen, G. (1996) On the use of thiol-modifying agents to determine channel topology, *Neuropharmacology 35*, 797−804.
66. Phoenix, D. A., Harris, F., Daman, O. A., and Wallace, J. (2002) The prediction of amphiphilic α-helices, *Curr. Protein Pept. Sci. 3*, 201−221.
67. Seol, W., and Shatkin, A. J. (1993) Membrane topology model of *Escherichia coli* α-ketoglutarate permease by PhoA fusion analysis, *J. Bacteriol. 175*, 565−567.
68. Lemieux, M. J., Huang, Y., and Wang, D.-N. (2004) The structural basis of substrate translocation by the *Escherichia coli* glycerol-3-phosphate transporter: A member of the major facilitator superfamily, *Curr. Opin. Struct. Biol. 14*, 405−412.
69. Abramson, J., Kaback, H. R., and Iwata, S. (2004) Structural comparison of the lactose permease and the glycerol-3-phosphate antiporter: Members of the major facilitator superfamily, *Curr. Opin. Struct. Biol. 14*, 413−419.
70. Krämer, R., and Morbach, S. (2004) BetP of *Corynebacterium glutamicum*, a transporter with three different functions: Betaine transport, osmosensing, and osmoregulation, *Biochim. Biophys. Acta 1658*, 31−36.
71. Peter, H., Weil, B., Burkovski, A., Krämer, R., and Morbach, S. (1998) *Corynebacterium glutamicum* is equipped with four secondary carriers for compatible solutes: Identification, sequencing, and characterisation of the proline/ectoine uptake system ProP and the ectoine/proline/glycine betaine carrier EctP, *J. Bacteriol. 180*, 6005−6012.

BI047383O